Late Eemian warming in the Nordic Seas as seen in proxy data and climate models

A. Born,[1,2,3,4] K. H. Nisancioglu,[1,5] and B. Risebrobakken[1,5]

Received 6 July 2010; revised 26 November 2010; accepted 2 February 2011; published 22 April 2011.

[1] We analyze a transient simulation of the last glacial inception in a climate model of intermediate complexity, focusing on sea ice–ocean circulation dynamics in the North Atlantic and Nordic Seas. As northern high-latitude summer insolation decreases toward the end of the Eemian interglacial, Arctic sea ice export to the North Atlantic increases. This surface fresh water transport weakens deep water formation in the North Atlantic and the near-surface circulation of the subpolar gyre. As a consequence, the relative contribution of subpolar gyre waters to the Atlantic inflow into the Nordic Seas is reduced, giving way to more warm and saline subtropical waters from the North Atlantic Current. We thus find an episode of relatively high heat and salt transport into the Nordic Seas during the last glacial inception between 119,000 and 115,000 years before present. This stabilizes deep ocean convection in the region and warms Scandinavia during a phase of low insolation. These findings are in good agreement with proxy data from the Nordic Seas and North Atlantic. At the end of the warm interval, sea surface temperature drops by about 3°C, marking the onset of large-scale glacier growth over Scandinavia.

Citation: Born, A., K. H. Nisancioglu, and B. Risebrobakken (2011), Late Eemian warming in the Nordic Seas as seen in proxy data and climate models, *Paleoceanography*, *26*, PA2207, doi:10.1029/2010PA002027.

1. Introduction

[2] The last glacial inception about 115,000 years ago (115 ka) was a period of exceptionally low summer insolation in northern high latitudes. This facilitated the nucleation of continental-scale ice sheets in the Northern Hemisphere and triggered feedback processes which eventually led to the end of the interglacial climate and a shift to a cold glacial climate [*de Noblet et al.*, 1996; *Khodri et al.*, 2001; *Calov et al.*, 2005].

[3] There is, however, evidence that the cooling due to lower insolation was not homogeneous and that relatively high temperatures prevailed in the eastern North Atlantic [*Chapman and Shackleton*, 1999; *Bauch and Kandiano*, 2007] and the eastern and northern Nordic Seas [*Risebrobakken et al.*, 2007] throughout the insolation minimum. The warming is attributed to a strengthening of the Norwegian Atlantic Current (NwAC), carrying warm and saline water from the Atlantic Ocean through the Nordic Seas into the Barents Sea and Arctic Ocean (Figure 1). It plays an important role in the formation of deep waters and changes in its strength likely impact the deep outflow from the Nordic Seas. A weakening of this deep current only after the insolation minimum also suggests that the NwAC continued to be active [*Rasmussen et al.*, 1999]. Further south, in the central North Atlantic, a northward shift of the North Atlantic Current is reported coeval with the strengthening of the NwAC [*Cortijo et al.*, 1999]. The combined evidence from proxy data thus indicates a reorganization of the large-scale current system.

[4] Previous modeling work identified the following chain of events in the Institut Pierre-Simon Laplace coupled climate model version 4 (IPSL CM4) [*Born et al.*, 2010]: decreased summer insolation in northern high latitudes at 115 ka compared to 126 ka increases the Arctic sea ice volume. Thus, thicker sea ice is transported southward in the East Greenland Current, freshening the surface waters of the North Atlantic. Consequently, deep convection is shut down in this region and the altered density structure weakens the subpolar gyre. This in turn reduces the relative contribution of the subpolar gyre to a water mass formed in the Rockall region of the eastern North Atlantic, giving way to more warm and saline subtropical waters to enter the Nordic Seas [*Hátún et al.*, 2005]. This mechanism counteracts decreasing insolation and the general freshening trend due to enhanced sea ice transport (Figure 2). The weaker subpolar gyre also allows for a northward shift of the North Atlantic Current, observed as a warm anomaly and a salinity dipole off Newfoundland.

[5] In the present study we expand this work with a transient simulation. The aim is to investigate if findings from proxy data can be reproduced in a physically consistent climate model and thus provide a detailed description of the regional climate evolution of the last glacial inception.

[1]Bjerknes Centre for Climate Research, Bergen, Norway.
[2]Geophysical Institute, University of Bergen, Bergen, Norway.
[3]Potsdam Institute for Climate Impact Research, Potsdam, Germany.
[4]Now at Climate and Environmental Physics, Physics Institute, University of Bern, Bern, Switzerland.
[5]Uni Bjerknes Centre, Bergen, Norway.

0883-8305/11/2010PA002027

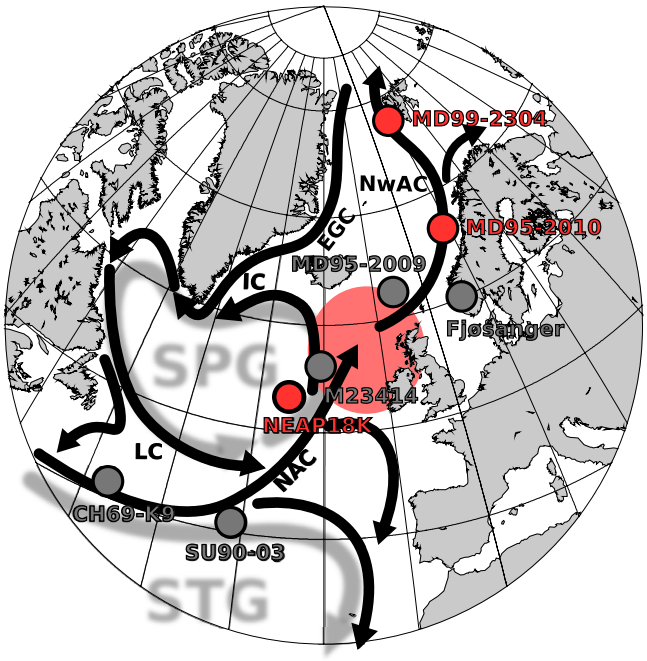

Figure 1. Map of the North Atlantic and Nordic Seas showing major ocean surface currents (arrows), marine sediment cores used in this study (red), and marine sediment cores and a terrestrial excavation site discussed in the text (gray). See Table 1 for references. Current systems of subpolar gyre (SPG) and subtropical gyre (STG) are illustrated in light gray. Source region of NwAC is highlighted in light red. Abbreviations are NAC, North Atlantic Current; NwAC, Norwegian Atlantic Current; EGC, East Greenland Current; LC, Labrador Current; and IC, Irminger Current.

The North Atlantic surface circulation is found to play an important role. Because simulations of such long time intervals can only be carried out at the expense of spatial detail, we will complement these results with high-resolution time slice simulations of a different model. Following a description of models in section 2 and proxy data in section 3, results of the two coupled climate models are analyzed in section 4. Based on the model results, an interpretation and discussion of proxy data is given in section 5. We summarize and conclude in section 6.

2. Model Description and Experiments

[6] This study combines simulations of a high-resolution ocean atmosphere general circulation model, IPSL CM4 [*Marti et al.*, 2010], and a coupled climate model of intermediate complexity CLIM*BER*-3α [*Montoya et al.*, 2005]. Time slice experiments have been carried out for 126 ka and 115 ka in both models, and integrated to quasi-equilibrium. In addition, a transient simulation with CLIM*BER*-3α was integrated from the end of the 126 ka equilibrium with variable orbital forcing through 110 ka. A series of sensitivity experiments with CLIM*BER*-3α is used to test the model's response to anomalous freshwater flux at 126 ka.

[7] Despite their differences, both models simulate the same dynamical changes at the last glacial inception. This allows us to combine their respective strengths and to discuss both temporal and spatial variations in the proxy data record effectively. The transient simulation of the entire time interval establishes a succession of events that forms the basis for comparison of the detailed time slice simulations with proxy data. Comparing time slice simulations with proxy data would otherwise be problematic due to large dating uncertainties in the data of the order of 5000 years [*Martinson et al.*, 1987].

[8] All experiments are forced by orbital insolation following *Berger* [1978] and fixed greenhouse gas concentrations at the preindustrial level (CO_2, 280 ppmv). The latter is a good approximation for the Eemian and the last glacial

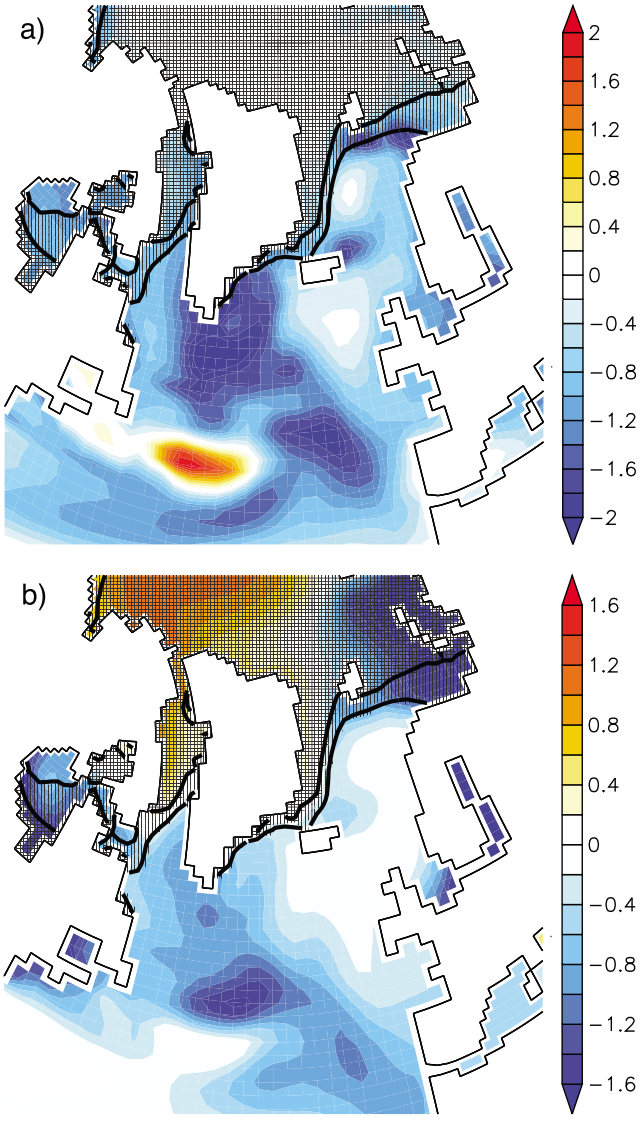

Figure 2. Differences between 115 ka and 126 ka for IPSL CM4, averaged over the upper 50 m; (a) temperature in degrees Celsius and (b) salinity in psu. Areas covered by more than 50% sea ice annually averaged are hatched horizontally (126 ka) and vertically (115 ka) to mask regions directly affected by sea ice. Temperature and salinity show almost no change in the NwAC source region in the eastern North Atlantic and along the path of the Atlantic inflow into the Nordic Seas.

Table 1. Locations of Marine Sediment Cores Used or Discussed in the Text[a]

Core Name	Position	Depth (m)	References
MD99-2304	78°N, 10°E	1315	*Risebrobakken et al.* [2005, 2007]
MD95-2010	67°N, 5°E	1226	*Risebrobakken et al.* [2005, 2007]
MD95-2009	63°N, 4°W	1027	*Rasmussen et al.* [1999]
Fjøsanger	60°N, 5°E	0	*Mangerud et al.* [1981]
M23414	54°N, 20°W	2196	*Bauch and Kandiano* [2007]
NEAP18K	52°N, 30°W	3275	*Chapman and Shackleton* [1999], *Cortijo et al.* [1999]
CH69-K9	41°N, 47°W	4100	*Cortijo et al.* [1999]
SU90-03	40°N, 32°W	2475	*Cortijo et al.* [1999]

[a]Original references to previously published proxy records are given.

inception until about 112 ka [*Petit et al.*, 1999; *Lüthi et al.*, 2008]. CO_2 concentration started decreasing gradually at 112 ka, reaching 250 ppmv at 110 ka. This is not included in the simulations. However, this only concerns the very last part of the studied interval. Details of the models and relevant references are given below.

2.1. IPSL CM4

[9] The Institut Pierre Simon Laplace coupled model version 4 (IPSL CM4) comprises ocean, sea ice, atmosphere and land surface components. The ocean model's dynamical core is based on the OPA system [*Madec et al.*, 1997]. The configuration used here (ORCA2) uses a horizontal resolution based on a 2° Mercator mesh, enhanced to 0.5° meridional resolution near the equator for a better representation of the equatorial wave channel. Two poles are placed over continents in the Northern Hemisphere in order to avoid a singularity in the Arctic Ocean. There are 31 unevenly spaced levels in the vertical. A free surface formulation is used for the upper boundary [*Roullet and Madec*, 2000], and a diffusive boundary parametrization is used for the bottom [*Beckmann*, 1998].

[10] The dynamic sea ice model (LIM2) [*Fichefet and Maqueda*, 1997, 1999] uses the horizontal ocean grid to compute ice rheology and advection. Thermodynamics are computed in three vertical layers, the uppermost for snow. Ice growth and melting are determined by an energy balance at both the snow-ice and water-ice boundary and in leads. Internal forces follow a viscous-plastic law [*Hibler*, 1979]. The model features parametrizations for the trapping of shortwave radiation by brine pockets, leads in the ice, as well as an implicit representation of subgrid variations in snow and ice thickness.

[11] The atmosphere is modeled by a comprehensive general circulation model (LMDZ) [*Hourdin et al.*, 2006] with a resolution of 3.75 zonally and 2.5 meridionally on 19 vertical levels. Precipitation over land is returned to the ocean by means of a river routing scheme implemented in the land surface model (ORCHIDEE) [*Krinner et al.*, 2005].

[12] The simulations for 126 ka and 115 ka were initiated with an ocean at rest and preindustrial hydrography [*Levitus*, 1982] and integrated for 300 and 800 years, respectively. The results presented are calculated from averages over the last 100 years of the simulations. More information on the simulations can be found in the works by *Braconnot et al.* [2008] and *Born et al.* [2010].

2.2. CLIM*BER*-3α

[13] CLIM*BER*-3α consists of the statistical-dynamical atmospheric model POTSDAM-2 [*Petoukhov et al.*, 2000] coupled to a global, 24-layer ocean general circulation model based on the Geophysical Fluid Dynamics Laboratory (GFDL) Modular Ocean Model version 3 (MOM-3) code and to the dynamic and thermodynamic sea ice module of *Fichefet and Maqueda* [1997]. The sea ice component is based on the same code-base as in IPSL CM4. The oceanic horizontal resolution is 3.75° × 3.75°. We apply a weak background vertical diffusivity of 0.2×10^{-4} m^2/s. For a discussion of the model's sensitivity to this parameter refer to *Mignot et al.* [2006]. Sea ice albedo is increased by 5% compared to *Montoya et al.* [2005] in order to ensure a more realistic Arctic sea ice cover at 126 ka. This change is within uncertainties of observed ice albedo values.

[14] The atmospheric model has a coarse spatial resolution (7.5° in latitude and 22.5° in longitude) and is based on the assumption of a universal vertical structure of temperature and humidity, which allows reducing the three-dimensional description to a set of two-dimensional prognostic equations. Heat and freshwater fluxes between the ocean and the atmosphere are computed on the oceanic grid and applied without flux adjustments. The wind stress is computed as the sum of the NCEP-NCAR reanalysis wind stress climatology [*Kalnay et al.*, 1996] and the wind stress anomaly calculated by the atmospheric model relative to a preindustrial control run. This model has been used in several studies of past climates [*Montoya et al.*, 2010; *Born and Levermann*, 2010] and future projections [*Feulner and Rahmstorf*, 2010] as well as in model intercomparisons [*Gregory et al.*, 2005; *Stouffer et al.*, 2006; *Levermann et al.*, 2007].

[15] Time slice experiments for 126 ka and 115 ka were initialized from the preindustrial control experiment and run to equilibrium for more than 2000 years. A transient simulation was started from the equilibrium of the 126 ka experiment and ran through 110 ka. Atmospheric chemical composition, land surface topography and albedo were fixed and thus neglect feedbacks of the progressing glacial inception. However, as discussed in section 6, findings presented here do not depend critically on this simplification. A control experiment with forcing fixed at 126 ka was run in parallel for 4000 years. In order to test the model's sensitivity to increased sea ice export, a series of experiments was carried out with anomalous freshwater flux south of Denmark Strait. These experiments are based on the 126 ka equilibrium and run to equilibrium for 2000 years.

3. Marine Sediment Cores and Proxy Data

[16] Marine proxy records from cores MD99-2304 (eastern Fram Strait), MD95-2010 (Vøring Plateau) and NEAP18K (Rockall Plateau) are presented (Figure 1). The cores are located along the pathway of Atlantic water toward the Arctic. From MD99-2304 and MD95-2010 relative abundances of *Neogloboquadrina pachyderma* (sin) and *Neogloboquadrina pachyderma* (dex) are shown, as well as calculated sea surface temperatures. Planktic $\delta^{18}O$ of *Globigerina bulloides* and transfer function based sea surface temperatures are shown from NEAP18K. All records, except from the temperatures of MD99-2304 and MD95-2010, are previously published. Detailed information on methods and establishment

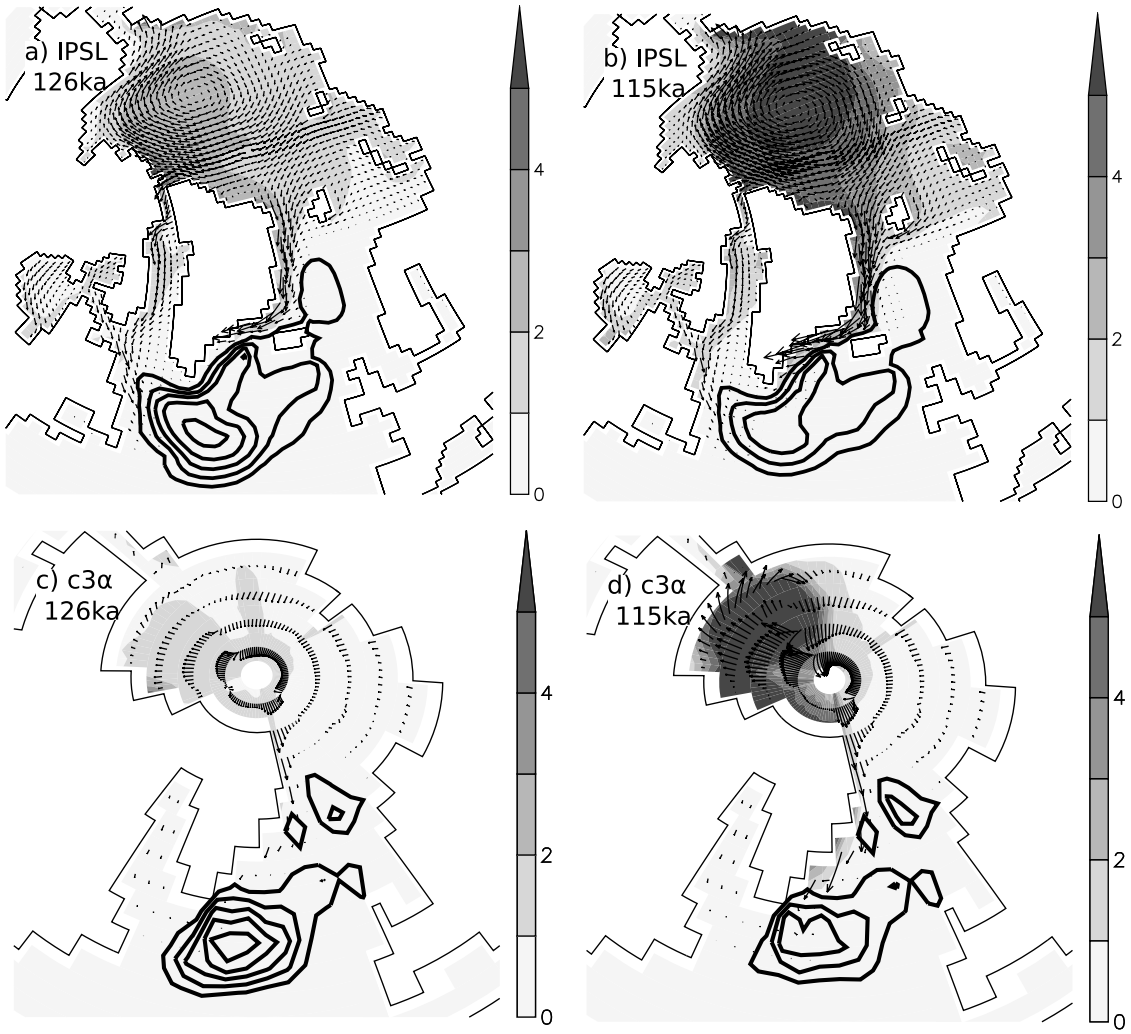

Figure 3. Arctic sea ice thickness (shading, in meters), sea ice volume transport per meter (arrows, in square meters per second), and depth integrated stream function (contours, spacing 2 Sv, cyclonic flow only). (a and b) IPSL CM4; (c and d) CLIM*BER*-3α. Figures 3a and 3c are 126 ka, and Figures 3b and 3d are 115 ka. Both models agree well on sea ice thickening in the Arctic Ocean, more sea ice export in the East Greenland Current, and the consequential weakening of the subpolar gyre circulation.

of chronologies can be found in the original publications (Table 1). The chronology of NEAP18K is taken from *Chapman and Shackleton* [1999] and was also used as a master chronology when the chronologies of MD99-2304 and MD95-2011 were established by *Risebrobakken et al.* [2005]. The summer sea surface temperatures of MD99-2304 and MD95-2010 have been calculated based on the relative abundances of *N. pachyderma* (sin) ($T = -0.07 \cdot$ (%*N. pachyderma* (sin)) + 12.5) [*Johannessen*, 1987]. This equation is restricted by an upper and lower temperature limit of 5.5°C and 12.4°C, respectively. The amplitude of our sea surface temperature estimates may be affected, most probably by providing too warm temperatures in the cold end.

4. Model Results

4.1. Simulation of the Last Glacial Inception

[17] While resolution is significantly lower in CLIM*BER*-3α compared to IPSL CM4, the key elements determining the dynamical changes depend on large-scale features of the climate system and are thus well reproduced (Figure 3). At 126 ka, most of the Arctic winter sea ice is thinner than 3 m in IPSL CM4, and thinner than 2 m in CLIM*BER*-3α. Both models simulate a similar area of winter sea ice exceeding 5 m thickness at 115 ka. Sea ice volume transport through Denmark Strait increases in both models; by 53 mSv in IPSL CM4 and 23 mSv in CLIM*BER*-3α (1 Sv = 10^6 m^3/s). The subpolar gyre weakens from 26 Sv to 18 Sv between 126 ka and 115 ka in IPSL CM4 and from 29 Sv to 19 Sv in CLIM*BER*-3α.

[18] Analysis of the transient experiment supports the following causal chain led by changes in summer insolation (Figure 4). Arctic sea ice export through Denmark Strait increases as summer insolation decreases. The associated freshwater transport reduces the density in the subpolar gyre center (40°W–30°W, 53°N–57°N) and weakens the cyclonic circulation first gradually and after 119 ka in a rapid transition. Temperature changes in the subpolar gyre due to

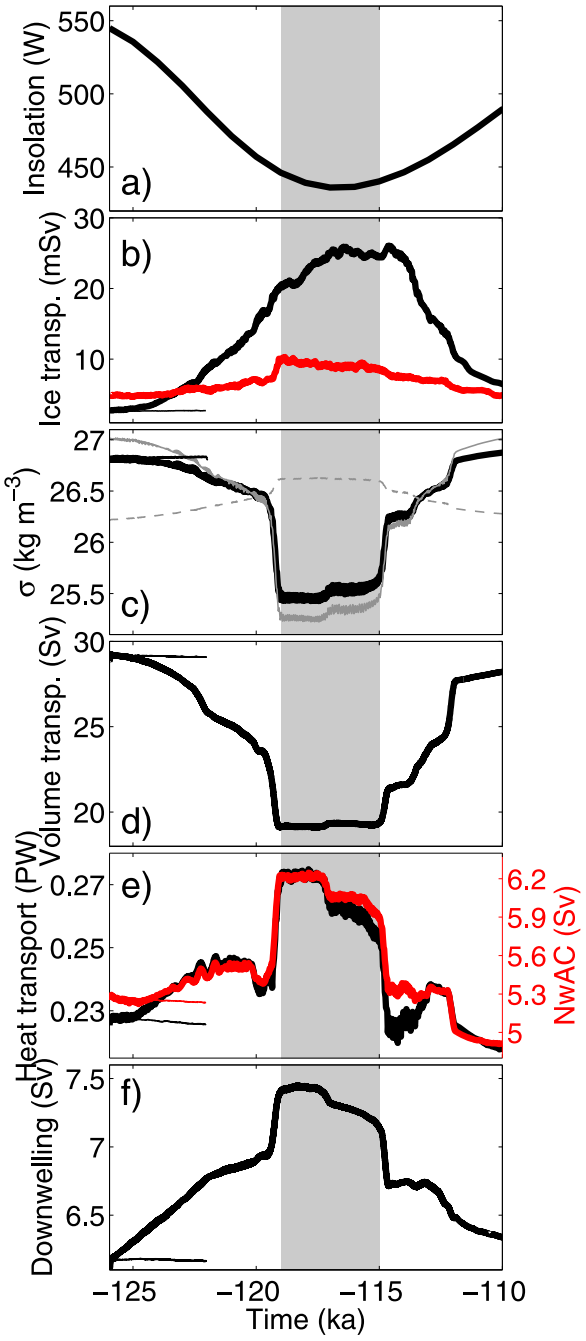

Figure 4. Key variables for climate evolution of the last glacial inception, averaged over 100 years, for CLIM*BER*-3α. Thin curves show results of a 126 ka control experiment. Gray shading highlights the period of maximum heat transport (compare to Figure 8). (a) June insolation at 65°N; (b) southward sea ice transport through Denmark Strait (black) and net air-sea freshwater flux in the subpolar gyre center (red, positive into ocean); (c) surface density in the subpolar gyre center (black), decomposed into salinity (gray solid line) and temperature (gray dashed line) contributions; (d) circulation strength of the subpolar gyre; (e) heat transport (black) and volume transport (red) in the NwAC across a zonal section at 64°N; and (f) downwelling in the Nordic Seas.

the changing insolation forcing are minor and cause only a small density signal. Changes in the freshwater exchange with the atmosphere are smaller than those due to import of freshwater by sea ice and are mostly due to changes in evaporation. Thus, they can be attributed to lower sea surface temperatures in the subpolar gyre center caused by the reorganization of the circulation (also seen in IPSL CM4, Figure 2a). Consistent with this view, the air-sea freshwater balance changes rapidly coeval with the subpolar gyre index and is a response to, rather than a cause of the observed changes. Concurrent with the change in circulation, northward heat transport by the NwAC increases by 16% (~39 × 10^{12} W). As summer insolation increases again the process is reversed with a second abrupt transition at 115 ka.

[19] Besides the external forcing by Arctic sea ice export, positive feedback mechanisms inherent to the subpolar gyre amplify the density changes in its center, leading to the abrupt transitions at 119 ka and 115 ka. The subpolar gyre is partly controlled by the density gradient between its center and rim. As the gyre and the Irminger current, its northeastern limb, weaken at 119 ka, they transport less salt from the relatively saline eastern into the fresher western subpolar North Atlantic, further reducing the density at the gyre's center. The result is an abrupt decrease in density in response to the gradually increasing freshwater transport by sea ice (Figure 4c). In addition to the salt signal, reduced convection due to the more buoyant surface waters (Figure 5) leads to a subsurface warming which further reduces the density (not shown). These mechanisms have been shown to operate in IPSL CM4 [*Born et al.*, 2010] and in CLIM*BER*-3α [*Levermann and Born*, 2007].

[20] The increase in heat transport in CLIM*BER*-3α is in good agreement with the relative warming and salinification of the NwAC found in IPSL CM4 (Figure 2). Relatively warm sea surface temperatures are simulated by both models for the eastern North Atlantic on Rockall Plateau (Figure 2a and Figure 8d). Note that despite increased heat transport by the NwAC, no absolute warming of the Nordic Seas is expected at 115 ka because of the counteracting large insolation forcing (Figure 4a). Similarly, enhanced salt transport counteracts the general freshening by sea ice locally but does not reverse it. However, this is enough to stabilize deep water formation in the Nordic Seas (Figure 4f) [*Born et al.*, 2010].

[21] Because of its coarse resolution, the estuarine circulation of the Nordic Seas is not represented accurately in CLIM*BER*-3α. The consequences of higher heat transport into the Nordic Seas for sea surface temperatures cannot be traced northward from the Greenland-Scotland ridge. This does not affect the findings above that are based entirely on the circulation south of the Greenland-Scotland ridge. Although not directly comparable, fluxes across the Greenland-Scotland ridge in CLIM*BER*-3α are generally similar to present-day observations by *Hansen and Østerhus* [2000]: about 7 Sv of Atlantic water and 0.25 PW of heat enter the Nordic Seas in the surface currents between Iceland and Scotland. This is approximately the same section used for the model in Figure 4e. Observed sinking in the Nordic Seas is about 6 Sv.

[22] Stabilization of Nordic Seas deep water formation is also seen in mixed layer depth (Figure 5). Deep convection remains active in the Nordic Seas despite the general surface freshening and more extensive sea ice (Figure 2b). Absolute

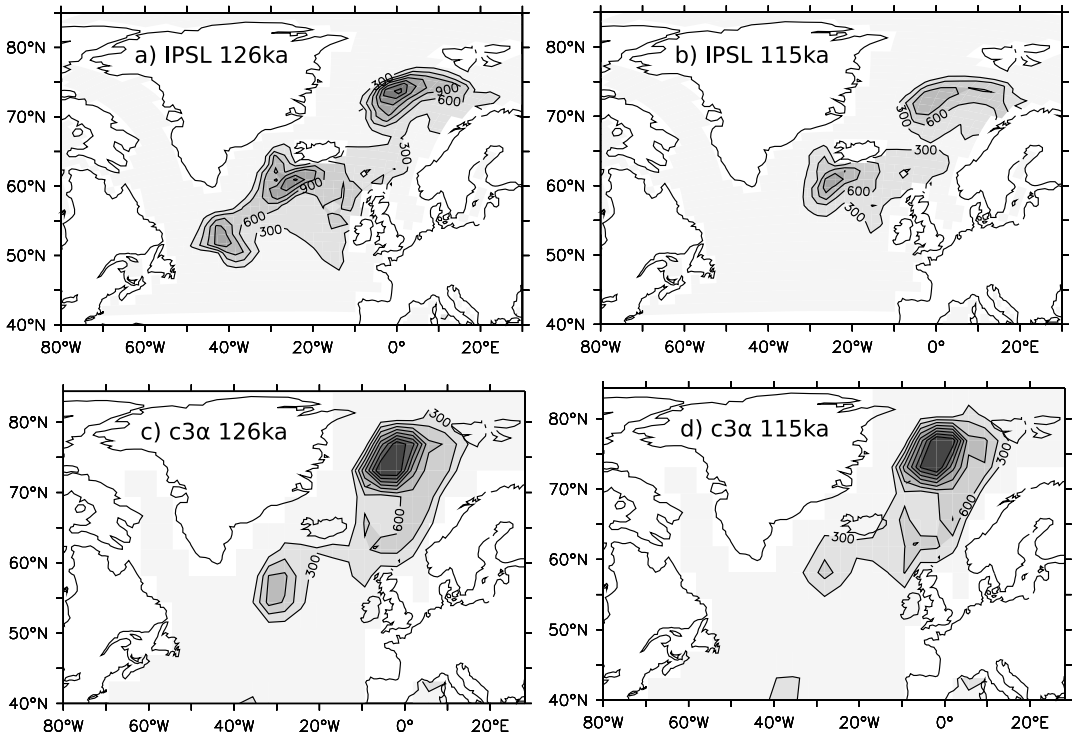

Figure 5. Mixed layer depth (in meters): (a and b) IPSL CM4 and (c and d) CLIM*BER*-3α. Figures 5a and 5c are 126 ka; Figures 5b and 5d are 115 ka. Deep convection in the Nordic Seas remains active at 115 ka in both models. South of the Greenland-Scotland ridge, convection decreases, leading to the shutdown of one convection region in IPSL CM4.

values differ between the two models. IPSL CM4 simulates a shallower mixed layer than CLIM*BER*-3α. Besides slightly different definitions of the mixed layer complicating a direct comparison, it is possible that the high-resolution IPSL CM4 model requires a longer integration time to equilibrate the deep ocean with possible impact on the formation of deep water. At the same time, a known deficiency of coarse resolution models is the imperfect representation of the southward outflow from the Nordic Seas over the deep and narrow sills of the Greenland-Scotland ridge that also influences the mixed layer depth [*Roberts and Wood*, 1997; *Thorpe et al.*, 2004; *Born et al.*, 2009]. As a result bottom waters leaving the Nordic Seas are less dense than observed and the reservoir of deep dense water in the Nordic Seas is not optimally represented in coarse resolution models which again impacts deep convection. The main conclusion, however, a stable deep circulation in the Nordic Seas at 115 ka, is consistent with both models. South of the Greenland-Scotland ridge, IPSL CM4 shows two deep convection regions of which only one is active at 115 ka. CLIM*BER*-3α does not resolve two distinct regions but shows a weaker convection at 115 ka. This is a result of freshening in both models (Figures 2b and 4c), caused by the enhanced sea ice transport into the region but partly also due to weaker salt advection in the subpolar gyre [*Levermann and Born*, 2007; *Born et al.*, 2010].

4.2. Sensitivity Experiments

[23] In order to test quantitatively how the increased Arctic sea ice export impacts the subpolar gyre, a series of experiments was carried out with CLIM*BER*-3α, simulating the redistribution of freshwater between the Arctic Ocean and a region south of Denmark Strait with anomalous fluxes of different strength, based on the 126 ka equilibrium experiment (Figure 6). The freshwater forcing was applied

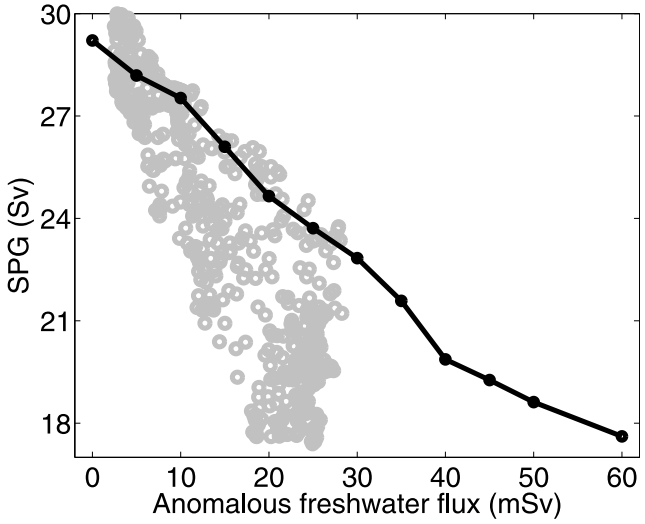

Figure 6. Equilibrium subpolar gyre strength at 126 ka as a function of anomalous freshwater flux south of Denmark Strait (black line) for CLIM*BER*-3α forcing region shown in Figure 7. Open gray circles show response of the subpolar gyre to sea ice transport through Denmark Strait in the transient experiment (see Figures 4b and 4d).

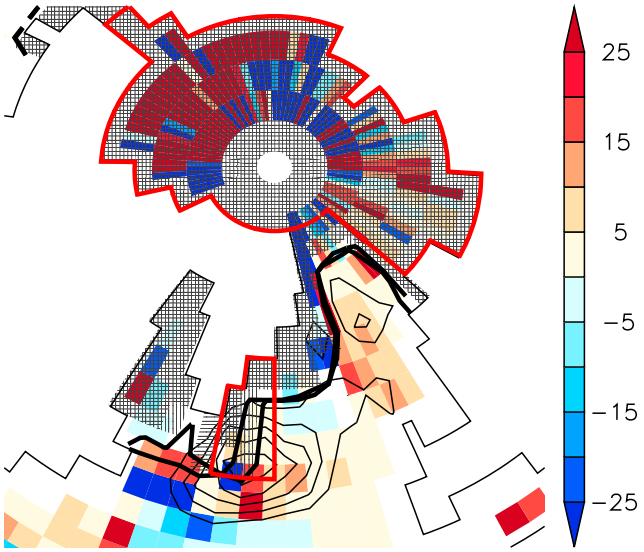

Figure 7. Relative changes in wind stress curl 115 ka minus 126 ka in the Arctic Ocean, Nordic Seas, and North Atlantic (colors, in percent) and annual average 15% sea ice area hatched horizontally (126 ka) and vertically (115 ka) for CLIM*BER*-3α. The depth integrated stream function at 126 ka is given for orientation (contours, spacing 5 Sv, cyclonic flow only). Regions used for the anomalous freshwater forcing are shown in red. Changes in the subpolar gyre region indicate a 1.3% strengthening of the cyclonic circulation while the subpolar gyre actually weakens by 34%.

continuously with no seasonal cycle. The experiments were run to equilibrium for 2100 years. Results shown are averages of the last 100 years. The subpolar gyre weakens rapidly to 19 Sv when an anomalous freshwater flux of 40 mSv is applied. This compares well to the reduction of the subpolar gyre to 19 Sv when the freshwater flux from sea ice equals 27 mSv in the transient experiment (Figure 4), supporting the hypothesis that increased Arctic sea ice export is the primary cause for the weaker gyre.

[24] There are several factors accounting for the weaker response of the subpolar gyre in the sensitivity experiments. The anomalous freshwater forcing was applied continuously while the freshwater transport by sea ice is stronger in winter and spring. The latter has a stronger impact on convection, which also occurs in late winter and plays an important role for the density structure of the deep water column and thus the subpolar gyre. Contrary to sea ice melt, the anomalous freshwater flux was distributed evenly over the region south of Denmark Strait. The impact of the precise location and timing of freshwater forcing on the subpolar gyre is an interesting topic in itself and worthy of investigation, but beyond the scope of this study.

[25] In addition to changes in buoyancy forcing, winds changed between 126 ka and 115 ka resulting in a stronger wind stress curl over the subpolar gyre (Figure 7). The average anomaly over the subpolar gyre (45°W–15°W, 45°N–63°N) indicates a 1.3% strengthening of the atmospheric cyclonic circulation compared to the 34% weakening of the subpolar gyre circulation. Large differences are found around the sea ice edge. In addition to the analysis shown for IPSL CM4 by *Born et al.* [2010], this suggests that the buoyancy forcing dominates the weakening.

5. Evidence of Strong Norwegian Atlantic Current From Proxy Data

[26] Our model experiments compare well to a number of marine proxy records throughout the North Atlantic and Nordic Seas (Figure 1 and Table 1). The simulation shows that maximum heat transport by the NwAC occurs around the time of minimum northern high-latitude summer insolation, lasting from 119 ka until 115 ka, in good agreement with foraminiferal faunal data from the Vøring Plateau (MD95-2010, Figure 8b) and the slope of western Spitsbergen (MD99-2304, Figure 8a) [*Risebrobakken et al.*, 2007]. Relatively high occurrence of the subpolar species *N. pachyderma* (dex) and *Turborotalita quinqueloba* (not shown) and low levels of the polar species *N. pachyderma* (sin) mark the peak of the interglacial warmth in both cores between approximately 126 ka and 120 ka. As insolation decreases, the relative abundance of *N. pachyderma* (sin) increases until 119 ka, when the trend reverses. The interval between 119 ka and 115 ka represents a partial recurrence of the subpolar species and thus interglacial conditions in both cores. By reconstructing surface temperature from the relative abundance of *N. pachyderma* (sin) [*Johannessen*, 1987], the temperature drop following the transient warm phase is estimated to about 3°C on the Vøring Plateau and 1.2°C off western Spitsbergen.

[27] The late Eemian warming is also seen in many cores from the Norwegian Sea, and it has been argued for a late Eemian climatic optimum, with the most intense advection of Atlantic surface water between 118.5 ka and 116 ka [*Bauch and Erlenkeuser*, 2008]. Decreasing sea surface temperatures at 115 ka, probably due to a weaker inflow of Atlantic waters, are consistent with several marine records from the Nordic Seas [*Fronval et al.*, 1998; *Risebrobakken et al.*, 2005], and have been associated to the North Atlantic ocean cooling event C26 [*Müller and Kukla*, 2004].

[28] A warm pulse is also found on the Rockall Plateau (NEAP18K) at about 115 ka, both in transfer function sea surface temperature estimates based on foraminiferal assemblages and planktic δ^{18}O in the surface dwelling species *Globigerina bulloides* (Figure 8c) [*Chapman and Shackleton*, 1999]. These findings are supported by similar results seen in M23414 [*Bauch and Kandiano*, 2007]. This North Atlantic warmth supports the hypothesis that the warm pulse in the Nordic Seas originates in the North Atlantic and that it is related to increased meridional heat transport across the Greenland-Scotland ridge.

[29] This reappearance of warm sea surface conditions on Rockall Plateau is simulated in the transient model simulation (Figure 8d), establishing a relative timing between the proxy records and the model simulations. Sea surface temperatures in the Nordic Seas cannot be directly compared with the transient model simulation due to the coarse model resolution. They are, however, consistent with the high-resolution time slice simulations. Temperature reconstructions from the relative abundance of *N. pachyderma* (dex) are based on the assumption that foraminifera are a water

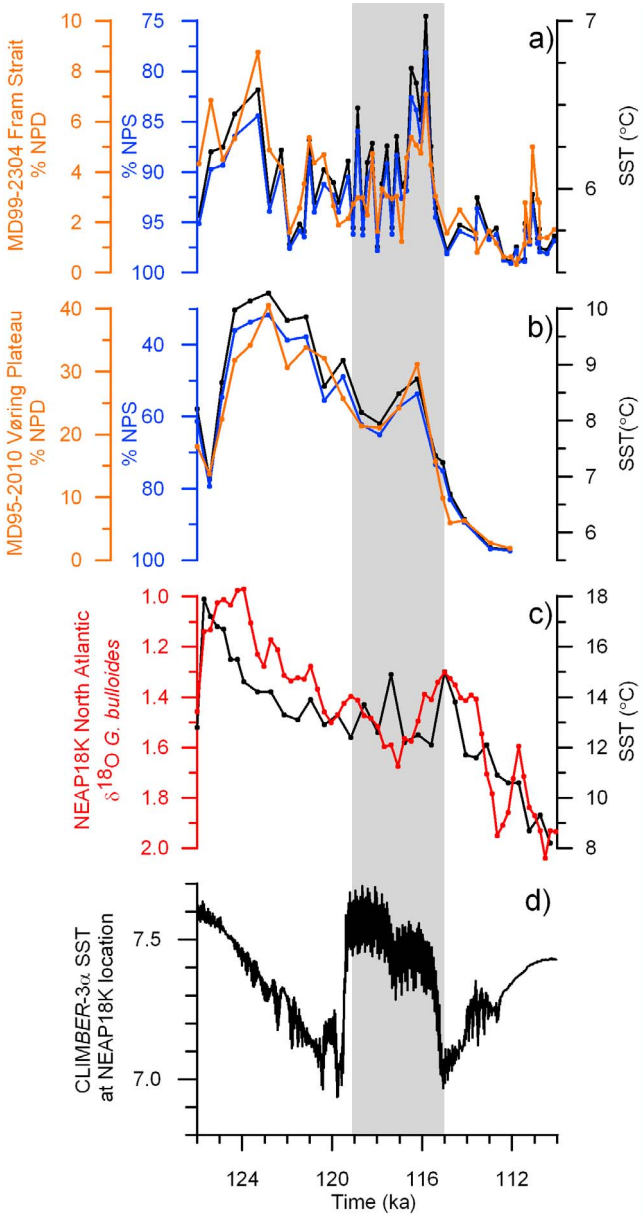

Figure 8. Proxy data reconstructions from the North Atlantic and Nordic Seas (see red dots in Figure 1). Gray shading highlights period of maximum simulated heat transport in the NwAC (Figure 4). (a) Relative abundance of *N. pachyderma* (sin) (blue) and *N. pachyderma* (dex) (orange) at the western Spitsbergen slope (MD99-2304) [*Risebrobakken et al.*, 2007]. Sea surface temperature estimate based on the relative abundance of *N. pachyderma* (sin) is shown in black [*Johannessen*, 1987]. (b) Same as Figure 8a but for the Vøring Plateau (MD95-2010). (c) *G. bulloides* δ^{18}O (red) (NEAP18K) [*Chapman and Shackleton*, 1999] and sea surface temperature estimate based on modern analog technique (black) [*Cortijo et al.*, 1999]. (d) Simulated temperature for CLIM*BER*-3α, averaged around the location of NEAP18K (32°W–28°W, 50°N–54°N, 0–100 m depth), averaged over 120 years (five points).

mass tracer. A relatively higher abundance of the warm-water subtype thus primarily indicates a stronger inflow of Atlantic water masses into the Nordic Seas, consistent with higher volume and heat transports. In this understanding, accounting for the original meaning of the proxy data, Figures 8b and 4e represent a direct comparison.

[30] The detailed time slice simulations with IPSL CM4 show surface warming off Newfoundland in the central North Atlantic (Figure 2a). As explained above, this is the result of a weaker subpolar gyre and a subsequent northward shift of the North Atlantic Current, providing additional means to test the dynamical hypothesis of this study with proxy data.

[31] Warmer and more saline water is seen during the late interglacial in the central North Atlantic (Figure 1, CH69-K9 and SU90-03), in reconstructions based on planktic foraminiferal assemblage data and planktic δ^{18}O [*Cortijo et al.*, 1999]. Generally, the prolonged warmth of the last interglacial, beyond the insolation minimum, is well documented for the eastern subpolar North Atlantic [*Ruddiman and McIntyre*, 1975; *McManus et al.*, 2002; *Oppo et al.*, 2006].

[32] In addition to the surface proxy data, evidence exists for a stable deep outflow from the Nordic Seas until 115 ka (MD95-2009) [*Rasmussen et al.*, 1999]. This outflow is fed by downwelling water masses in the Nordic Seas and thus corroborates the model simulation of an active deep circulation in the Nordic Seas (Figure 4f). A sharp decline in the supply to the densest part of North Atlantic Deep Water is also seen at the Bermuda rise at about the same time [*Hall et al.*, 1998;*Lehman et al.*, 2002], after adjusting the age model of *Lehman et al.* [2002] to the common age model of NEAP18K used in the present study [see *Risebrobakken et al.*, 2005].

[33] Warming toward the end of the Eemian interglacial can also be found in terrestrial data from southern Norway at Fjøsanger, indicated by the appearance of Ilex pollen (holly) [*Mangerud et al.*, 1981]. Thus, there is consistence also between our marine data and terrestrial evidence. Glaciation started soon after this final warm peak. Although the data from Fjøsanger cannot be strictly correlated with the marine cores, it suggests that a warming preceded imminent inception over Scandinavia and Spitsbergen. In an effort to correlate marine and terrestrial data of the last glacial inception on a common time scale, *Müller and Kukla* [2004] conclude that the cessation of the oceanic meridional heat transport into the Nordic Seas at 115 ka caused a substantial cooling of northern Europe and steeper vegetation and climate gradients over most of the continent.

6. Summary and Discussions

[34] We present a physical mechanism for enhanced warmth in the eastern subpolar North Atlantic and along the path of the NwAC during times of minimum insolation forcing 115,000 years before present. Increased Arctic sea ice export in the East Greenland Current, as a direct result of the lower insolation, triggers nonlinear dynamical feedbacks of the subpolar gyre, and leads to a weaker circulation. This in turn increases the fraction of relatively warm and saline subtropical waters entering the Nordic Seas. The resulting increase in heat and salt transport into the Nordic Seas stabilizes ocean circulation and climate of the region.

Comparison with marine sediment proxy data at the Fram Strait, Vøring Plateau and Rockall Plateau yields good agreement with model results.

[35] In addition to a warm eastern North Atlantic and Nordic Seas, the weaker subpolar gyre results in a northward shift of the North Atlantic Current, creating a warm anomaly in the central North Atlantic which can also be found in proxy data. This distinctive warming pattern is the fingerprint of a weaker subpolar gyre circulation at the last glacial inception. The combination of independent proxy data thus supports the dynamical hypothesis presented here.

[36] Intensification of the Atlantic meridional overturning circulation due to freshwater storage in growing ice sheets on land and decreased runoff into the ocean was found to be the reason for large-scale warming of the North Atlantic south of the Greenland-Scotland ridge during the last glacial inception [*Ruddiman and McIntyre*, 1975; *Labeyrie et al.*, 1999; *McManus et al.*, 2002; *Meissner and Gerdes*, 2002]. The North Atlantic remained warm for at least 5000 years after the Nordic Seas cooling *Müller and Kukla* [2004]. The mechanism presented here does not address the strengthening of the large-scale deep ocean circulation, but specifically the inflow into the Nordic Seas and consequences for the northernmost limb of the thermohaline circulation. The two different views are compatible.

[37] It was suggested that Labrador Sea deep convection was not active during the last interglacial [*Hillaire-Marcel et al.*, 2001; *Cottet-Puinel et al.*, 2004]. However, Labrador Sea water was produced throughout the Eemian, albeit probably at a weaker rate [*Evans et al.*, 2007] and associated to convection taking place further north in the Labrador Sea [*Rasmussen et al.*, 2003]. This is consistent with the simulations presented here.

[38] Several modeling studies identified the retreat of boreal forest and expansion of tundra with higher albedo as an important mechanism for glacier nucleation [*de Noblet et al.*, 1996; *Meissner et al.*, 2003; *Calov et al.*, 2005; *Kubatzki et al.*, 2006]. However, a feedback to ocean circulation was not reported, and the mechanism described here is unlikely to depend on changes in vegetation.

[39] The application of fixed present day ice sheet configuration probably introduces only negligible error to the simulation of the last glacial inception. The Eemian was very similar to present day with the Greenland ice sheet about 30% smaller, equivalent to approximately 3 m sea level rise [*Otto-Bliesner et al.*, 2006; *de Vernal and Hillaire-Marcel*, 2008]. Climate evolution was found to be insensitive to the exact choice of initial Greenland topography [*Kubatzki et al.*, 2006]. Global eustatic sea level declined approximately 40 m between 120 ka and 110 ka, indicating significant ice growth on land [*Waelbroeck et al.*, 2002]. However, the young ice sheets were probably relatively thin making their climatic effect little different from perennial snow fields which are included in the model used here.

[40] Both marine and terrestrial proxy data indicate that large-scale glacier growth started soon after the late Eemian warm phase [*Mangerud et al.*, 1981; *Baumann et al.*, 1995; *Risebrobakken et al.*, 2007], suggesting that the intrusion of Atlantic waters into the Nordic Seas played an important role for glacial inception over Scandinavia. Whether this warm water enhanced the air-sea temperature contrast, increased moisture transport, and accelerated ice growth, or rather delayed ice growth due to warming is unclear.

[41] **Acknowledgments.** We kindly acknowledge Pascale Braconnot for access to IPSL CM4 model output as well as discussions with Jan Mangerud, John Inge Svendsen, and Tore Furevik. The present work benefited greatly from comments by two anonymous reviewers that are gratefully acknowledged. A.B. was funded by the Marie Curie Actions project NICE (MRTN-CT-2006-036127) and the Research Council of Norway project TOPPNICE. Computer time was provided by the Research Council of Norway through the NOTUR project, Potsdam Institute for Climate Impact Research, Centre National de la Recherche Scientifique (IDRIS computing center), and the Commissariat à l'Energie Atomique (CCRT computing center). This is publication A314 from the Bjerknes Centre for Climate Research.

References

Bauch, H. A., and H. Erlenkeuser (2008), A "critical" climatic evaluation of last interglacial (MIS 5e) records from the Norwegian Sea, *Polar Res.*, *27*, 135–151.

Bauch, H. A., and E. S. Kandiano (2007), Evidence for early warming and cooling in North Atlantic surface waters during the last interglacial, *Paleoceanography*, *22*, PA1201, doi:10.1029/2005PA001252.

Baumann, K.-H., K. S. Lackschewitz, J. Mangerud, R. F. Spielhagen, T. C. W. Wolf-Welling, R. Henrich, and H. Kassens (1995), Reflection of Scandinavia ice sheet fluctuations in Norwegian Sea sediments during the last 150,000 years, *Quat. Res.*, *43*, 185–197.

Beckmann, A. (1998), The representation of bottom boundary layer processes in numerical ocean circulation models, in *Ocean Modeling and Parametrization*, edited by E. P. Chassignet and J. Verron, pp. 135–154, Kluwer Acad., Dordrecht, Netherlands.

Berger, A. (1978), Long-term variations of caloric solar radiation resulting from the Earth's orbital elements, *Quat. Res.*, *9*, 139–167.

Born, A., and A. Levermann (2010), The 8.2 ka event: Abrupt transition of the subpolar gyre toward a modern North Atlantic circulation, *Geochem. Geophys. Geosyst.*, *11*, Q06011, doi:10.1029/2009GC003024.

Born, A., A. Levermann, and J. Mignot (2009), Sensitivity of the Atlantic ocean circulation to a hydraulic overflow parameterisation in a coarse resolution model: Response of the subpolar gyre, *Ocean Modell.*, *27*, 130–142.

Born, A., K. H. Nisancioglu, and P. Braconnot (2010), Sea ice induced changes in ocean circulation during the Eemian, *Clim. Dyn.*, *35*, 1361–1371, doi:10.1007/s00382-009-0709-2.

Braconnot, P., C. Marzin, L. Grégoire, E. Mosquet, and O. Marti (2008), Monsoon response to changes in Earth's orbital parameters: comparisons between simulations of the Eemian and of the Holocene, *Clim. Past*, *4*, 281–294.

Calov, R., A. Ganopolski, V. Petoukhov, M. Claussen, V. Brovkin, and C. Kubatzki (2005), Transient simulation of the last glacial inception. Part II: Sensitivity and feedback analysis, *Clim. Dyn.*, *24*, 563–576.

Chapman, M. R., and N. J. Shackleton (1999), Global ice-volume fluctuations, North Atlantic ice-rafting events, and deep-ocean circulation changes between 130 and 70 ka, *Geology*, *27*, 795–798.

Cortijo, E., S. Lehman, L. Keigwin, M. Chapman, D. Paillard, and L. Labeyrie (1999), Changes in meridional temperature and salinity gradients in the North Atlantic Ocean (30°N–72°N) in the last interglacial period, *Paleoceanography*, *14*, 23–33.

Cottet-Puinel, M., A. J. Weaver, C. Hillaire-Marcel, A. de Vernal, P. U. Clark, and M. Eby (2004), Variation of Labrador Sea water formation over the Last Glacial cycle in a climate model of intermediate complexity, *Quat. Sci. Rev.*, *23*, 449–465.

de Noblet, N., I. Prentice, S. Joussaume, D. Texier, A. Botta, and A. Haxeltine (1996), Possible role of atmosphere-biosphere interactions in triggering the Last Glaciation, *Geophys. Res. Lett.*, *23*, 3191–3194.

de Vernal, A., and C. Hillaire-Marcel (2008), Nature variability of Greenland climate vegetation, and ice volume during the past million years, *Science*, *320*, 1622–1625.

Evans, H. K., I. R. Hall, G. G. Bianchi, and D. W. Oppo (2007), Intermediate water links to Deep Western Boundary Current variability in the subtropical NW Atlantic during marine isotope stages 5 and 4, *Paleoceanography*, *22*, PA3209, doi:10.1029/2006PA001409.

Feulner, G., and S. Rahmstorf (2010), On the effect of a new grand minimum of solar activity on the future climate on Earth, *Geophys. Res. Lett.*, *37*, L05707, doi:10.1029/2010GL042710.

Fichefet, T., and M. A. M. Maqueda (1997), Sensitivity of a global sea ice model to the treatment of ice thermodynamics and dynamics, *J. Geophys. Res.*, *102*, 12,609–12,646, doi:10.1029/97JC00480.

Fichefet, T., and M. A. M. Maqueda (1999), Modelling the influence of snow accumulation and snow-ice formation on the seasonal cycle of the Antarctic sea-ice cover, *Clim. Dyn.*, *15*, 251–268.

Fronval, T., E. Jansen, H. Haflidason, and J. P. Sejrup (1998), Variability in surface and deep water conditions in the Nordic seas during the last interglacial period, *Quat. Sci. Rev.*, *17*, 963–985.

Gregory, J. M., et al. (2005), A model intercomparison of changes in the Atlantic thermohaline circulation in response to increasing atmospheric CO_2 concentration, *Geophys. Res. Lett.*, *32*, L12703, doi:10.1029/2005GL023209.

Hall, I., I. McCave, M. Chapman, and N. Shackleton (1998), Coherent deep flow variation in the Iceland and American basins during the last interglacial, *Earth Planet. Sci. Lett.*, *164*, 15–21.

Hansen, B., and S. Østerhus (2000), North Atlantic–Nordic Seas exchanges, *Prog. Oceanogr.*, *45*, 109–208.

Hátún, H., A. B. Sandø, H. Drange, B. Hansen, and H. Valdimarsson (2005), Influence of the Atlantic subpolar gyre on the thermohaline circulation, *Science*, *309*, 1841–1844.

Hibler, W. D. (1979), A dynamic thermodynamic sea ice model, *J. Phys. Oceanogr.*, *9*, 815–846.

Hillaire-Marcel, C., A. de Vernal, A. Bilodeau, and A. J. Weaver (2001), Absence of deep-water formation in the Labrador Sea during the last interglacial period, *Nature*, *410*, 1073–1077.

Hourdin, F., et al. (2006), The LMDZ4 general circulation model: climate performance and sensitivity to parametrized physics with emphasis on tropical convection, *Clim. Dyn.*, *27*, 787–813.

Johannessen, T. (1987), Resente planktoniske foraminiferer fra Norskehavet, Islandhavet og Nordatlanteren: Taksonomi, faunafordeling og stabilisotopsammensetning, M.S. thesis, Universitetet i Bergen, Bergen, Norway.

Kalnay, E., et al. (1996), The NCEP/NCAR 40-year reanalysis project, *Bull. Am. Meteorol. Soc.*, *77*, 437–471.

Khodri, M., Y. Leclainche, G. Ramstein, P. Braconnot, O. Marti, and E. Cortijo (2001), Simulating the amplification of orbital forcing by ocean feedbacks in the last glaciation, *Nature*, *410*, 570–574.

Krinner, G., N. Viovy, N. de Noblet-Ducoudre, J. Ogee, J. Polcher, P. Friedlingstein, P. Ciais, S. Sitch, and I. C. Prentice (2005), A dynamic global vegetation model for studies of the coupled atmosphere-biosphere system, *Global Biogeochem. Cycles*, *19*(1), GB1015, doi:10.1029/2003GB002199.

Kubatzki, C., M. Claussen, R. Calov, and A. Ganopolski (2006), Sensitivity of the last glacial inception to initial and surface conditions, *Clim. Dyn.*, *27*, 333–344.

Labeyrie, L., H. Leclaire, C. Waelbroeck, E. Cortijo, J. C. Duplessy, L. Vidal, M. Elliot, and B. L. Coat (1999), Temporal variability of the surface and deep waters of the north west Atlantic Ocean at orbital and millenial scales, in *Mechanisms of Global Climate Change at Millennial Time Scales*, *Geophys. Monogr. Ser.*, vol. 112, edited by R. Webb, P. Clark, and L. Keigwin, pp. 77–88, AGU, Washington, D. C.

Lehman, S., J. Sachs, A. Crotwell, L. Keigwin, and E. Boyle (2002), Relation of subtropical Atlantic temperature, high-latitude ice rafting, deep water formation, and European climate 130,000–60,000 years ago, *Quat. Sci. Rev.*, *21*, 1917–1924.

Levermann, A., and A. Born (2007), Bistability of the Atlantic subpolar gyre in a coarse-resolution model, *Geophys. Res. Lett.*, *34*, L24605, doi:10.1029/2007GL031732.

Levermann, A., J. Mignot, S. Nawrath, and S. Rahmstorf (2007), The role of northern sea ice cover for the weakening of the thermohaline circulation under global warming, *J. Clim.*, *20*, 4160–4171.

Levitus, S. (1982), Climatological atlas of the world ocean, *NOAA Prof. Pap. 13*, 173 pp., U.S. Gov. Print. Off., Washington, D. C.

Lüthi, D., et al. (2008), High-resolution carbon dioxide concentration record 650,000–800,000 years before present, *Nature*, *453*, 379–382.

Madec, G., P. Delecluse, M. Imbard, and C. Lévy (1997), OPA version 8.1 Ocean General Circulation Model reference manual, *Note Pole Model. 11*, Institut Pierre-Simon Laplace, Paris.

Mangerud, J., E. Sønstegaard, H.-P. Sejrup, and S. Haldorsen (1981), A continuous Eemian-Early Weichelian sequence containing pollen and marine fossils at Fjøsanger, western Norway, *Boreas*, *10*, 138–205.

Marti, O., et al. (2010), Key features of the IPSL ocean atmosphere model and its sensitivity to atmospheric resolution, *Clim. Dyn.*, *34*, 1–26, doi:10.1007/s00382-009-0640-6.

Martinson, D. G., N. G. Pisias, J. D. Hays, J. Imbrie, T. C. Moore Jr., and N. J. Shackleton (1987), Age dating and the orbital theory of the ice ages: Development of a high-resolution 0 to 300,000-year chronostratigraphy, *Quat. Res.*, *27*, 1–29.

McManus, J. F., D. W. Oppo, L. D. Keigwin, J. L. Cullen, and G. C. Bond (2002), Thermohaline circulation and prolonged interglacial warmth in the North Atlantic, *Quat. Res.*, *58*, 17–21.

Meissner, K., and R. Gerdes (2002), Coupled climate modelling of ocean circulation changes during ice age inception, *Clim. Dyn.*, *18*, 455–473.

Meissner, K. J., A. J. Weaver, H. D. Matthews, and P. M. Cox (2003), The role of land surface dynamics in glacial inception: A study with the UVic Earth System Model, *Clim. Dyn.*, *21*, 515–537.

Mignot, J., A. Levermann, and A. Griesel (2006), A decomposition of the Atlantic meridional overturning circulation into physical components using its sensitivity to vertical diffusivity., *J. Phys. Oceanogr.*, *36*, 636–650.

Montoya, M., A. Griesel, A. Levermann, J. Mignot, M. Hofmann, A. Ganopolski, and S. Rahmstorf (2005), The Earth system model of intermediate complexity CLIMBER-3α. Part I: Description and performance for present-day conditions, *Clim. Dyn.*, *25*, 237–263.

Montoya, M., A. Born, and A. Levermann (2010), Reversed North Atlantic gyre dynamics in glacial climate, *Clim. Dyn.*, *36*, 1107–1118, doi:10.1007/s00382-009-0729-y.

Müller, U. C., and G. J. Kukla (2004), North Atlantic Current and European environments during the declining stage of the last interglacial, *Geology*, *32*, 1009–1012.

Oppo, D. W., J. F. McManus, and J. L. Cullen (2006), Evolution and demise of the Last Interglacial warmth in the subpolar North Atlantic, *Quat. Sci. Rev.*, *25*, 3268–3277.

Otto-Bliesner, B. L., S. J. Marshall, J. T. Overpeck, G. H. Miller, A. Hu, and CAPE Last Interglacial Project Members (2006), Simulating Arctic climate warmth and icefield retreat in the Last Interglaciation, *Science*, *311*, 1751–1753.

Petit, J. R., et al. (1999), Climate and atmospheric history of the past 420,000 years from the Vostok ice core, Antarctica, *Nature*, *399*, 429–436.

Petoukhov, V., A. Ganopolski, V. Brovkin, M. Claussen, A. Eliseev, C. Kubatzki, and S. Rahmstorf (2000), CLIMBER-2: A climate system model of intermediate complexity. Part I: Model description and performance for present climate, *Clim. Dyn.*, *16*, 1–17.

Rasmussen, T. L., E. Balbon, E. Thomsen, L. Labeyrie, and T. C. E. van Weering (1999), Climate records and changes in deep outflow from the Norwegian Sea 150–55 ka, *Terra Nova*, *11*, 61–66.

Rasmussen, T. L., D. W. Oppo, E. Thomsen, and S. J. Lehman (2003), Deep sea records from the southeast Labrador Sea: Ocean circulation changes and ice-rafting events during the last 160,000 years, *Paleoceanography*, *18*(1), 1018, doi:10.1029/2001PA000736.

Risebrobakken, B., T. Dokken, and E. Jansen (2005), The extent and variability of the Meridional Atlantic Circulation in the Nordic Seas during Marine Isotope Stage 5 and its influence on the inception of the last glacial, in *The Nordic Seas: An Integrated Perspective*, *Geophys. Monogr. Ser.*, vol. 158, edited by H. Drange et al., pp. 323–339, AGU, Washington, D. C.

Risebrobakken, B., T. Dokken, O. H. Otterå, E. Jansen, Y. Gao, and H. Drange (2007), Inception of the Northern European ice sheet due to contrasting ocean and insolation forcing, *Quat. Res.*, *67*, 128–135.

Roberts, M. J., and R. A. Wood (1997), Topographic sensitivity studies with a Bryan–Cox-type ocean model, *J. Phys. Oceanogr.*, *27*, 823–836.

Roullet, G., and G. Madec (2000), Salt conservation, free surface, and varying levels: A new formulation for ocean general circulation models, *J. Geophys. Res.*, *105*, 23,927–23,942.

Ruddiman, W. F., and A. McIntyre (1975), Warmth of the subpolar North Atlantic Ocean during Northern Hemisphere ice-sheet growth, *Science*, *204*, 173–175.

Stouffer, R. J., et al. (2006), Investigating the causes of the response of the thermohaline circulation to past and future climate changes, *J. Clim.*, *19*, 1365–1387.

Thorpe, R. B., R. A. Wood, and J. F. B. Mitchell (2004), Sensitivity of the modelled thermohaline circulation to the parameterisation of mixing across the Greenland-Scotland ridge, *Ocean Modell.*, *7*, 259–268.

Waelbroeck, C., L. Labeyrie, E. Michel, J. C. Duplessy, J. F. McManus, K. Lambeck, E. Balbon, and M. Labracherie (2002), Sea-level and deep water temperature changes derived from benthic foraminifera isotopic records, *Quat. Sci. Rev.*, *21*, 295–305.

A. Born, K. H. Nisancioglu, and B. Risebrobakken, Bjerknes Centre for Climate Research, Allégaten 55, N-5007 Bergen, Norway. (andreas.born@climate.unibe.ch)